

In situ studies of atomic, nano- and macroscale order during VOHPO₄·0.5H₂O transformation to (VO)₂P₂O₇

V.V. Guliant^{a,*}, S.A. Holmes^a, J.B. Benziger^b, P. Heaney^c, D. Yates^c, I.E. Wachs^d

^a Department of Chemical Engineering, University of Cincinnati, Cincinnati, OH 45221-0171, USA

^b Department of Chemical Engineering, Princeton University, Princeton, NJ 08544, USA

^c Department of Geology, Princeton University, Princeton, NJ 08544, USA

^d Department of Chemical Engineering, Zettlemoyer Center for Surface Studies, Lehigh University, Bethlehem, PA 18015, USA

Received 23 November 2000; accepted 14 March 2001

Abstract

Transformation of VOHPO₄·0.5H₂O precursor to well-crystallized (VO)₂P₂O₇, for *n*-butane oxidation to maleic anhydride was studied by in situ Raman and XRD techniques. Atomic scale changes observed in the precursor structure at 583 K provided new insights into its transformation to (VO)₂P₂O₇. In addition to (VO)₂P₂O₇, nanocrystalline oxidized δ-VOPO₄ invisible to XRD was detected during transformation in *n*-butane/air, possibly due to the specificity of the in situ conditions. Under catalytic reaction conditions the disordered nanocrystalline (VO)₂P₂O₇ in the fresh catalysts (ca. 10–20 nm domains) gradually transformed into well-crystallized (VO)₂P₂O₇ in the equilibrated VPO catalysts (>30 nm domains) with time on stream. Simultaneously, a disordered layer ca. 2 nm thick which was covering the surface (100) planes of (VO)₂P₂O₇ disappeared yielding a solid with high steady-state catalytic performance. Only (VO)₂P₂O₇ was observed both at room temperature and reaction temperature in the equilibrated VPO catalysts. Specific surface termination of the (100) planes of (VO)₂P₂O₇ in the equilibrated VPO catalysts is believed to be responsible for high activity and selectivity of these catalysts for maleic anhydride formation. © 2001 Elsevier Science B.V. All rights reserved.

Keywords: Vanadium pyrophosphate; In situ studies; Raman; XRD; Rietveld refinement

1. Introduction

Vanadyl(IV) hydrogen phosphate hemihydrate, VOHPO₄·0.5H₂O, is a precursor of the commercial vanadium-phosphorus-oxide (VPO) catalysts for partial oxidation of *n*-butane to maleic anhydride [1]. Vanadyl pyrophosphate, (VO)₂P₂O₇, obtained by the thermal transformation of the precursor phase has been identified as critical for the activity and selectivity of *n*-butane oxidation over the VPO catalysts [1–5]. The single crystal structures of VOHPO₄·0.5H₂O

and (VO)₂P₂O₇ have been recently elucidated in several studies [5–10]. The VOHPO₄·0.5H₂O and (VO)₂P₂O₇ phases possess similar crystal structures: the [VOHPO₄] layers are hydrogen-bonded via HPO₄²⁻ groups in the precursor phase [5,6] and become covalently bonded via pyrophosphate (P₂O₇⁴⁻) groups during the thermal transformation to vanadyl pyrophosphate [7–10]. On the macroscopic scale, the crystal morphology is preserved during this transformation. Several models for this so-called topotactic transformation of the precursor phase into vanadyl pyrophosphate have been previously proposed [11–14]. According to more recent models [11,12], the HPO₄ groups present in the precursor structure

* Corresponding author. Fax: +1-513-556-3473.
E-mail address: vguliant@alpha.che.uc.edu (V.V. Guliant).

are inadequately oriented to form the regular P–O–P linkages observed in the single crystal structure of $(VO)_2P_2O_7$ [7–10]. These recent transformation models involve either the concerted displacement of the hydrogen phosphate layers [12] or the inversion of the phosphate tetrahedra in the precursor phase to align the hydrogen phosphate groups sufficiently to form the pyrophosphate groups [11]. However, the former model [11] described a different P–O–P connectivity than the one established via single crystal diffraction studies [7–10]. On the other hand, the latter model [12] cannot account for several experimental observations: (i) the formation of a disordered intermediate during this transformation, which coexists with neither the starting nor product phases; (ii) the significant crystallographic disorder on the nanoscale; and (iii) the presence of extended defects in vanadyl pyrophosphate transformed under catalytic reaction conditions. These experimental observations indicate that the transformation process is more complex than suggested by the proposed models, and that the crystal structure of the catalytically active vanadyl pyrophosphate obtained at low temperatures (653–723 K) is much more disordered than the structure of single crystal vanadyl pyrophosphate obtained from the melt above 1173 K.

Hiroi et al. [15] suggested that there were in actuality two possible symmetries available for $(VO)_2P_2O_7$, depending on preparation conditions. Electron, X-ray and neutron diffraction studies on polycrystalline samples, prepared from the melt at 1023 K indicated the presence of solely orthorhombic material, space group $Pca2_1$. In this paper, defects were suggested to be attributable to the positional disorder of P_2O_7 groups, and that two distinct crystalline forms of $(VO)_2P_2O_7$ coexist with the same symmetry, or that one exists as a defect in the other.

The modeling of extended defects in the crystalline structure of vanadyl pyrophosphate has also been published recently [16]. These defects were proposed as being due to a bc stacking fault, i.e. a change in orientation from $-V=O-V=O-V=$ to $=V-O=V-O=V-$ at the stacking fault boundary. This was attributed to the incomplete dimerisation of the PO_3^{4-} groups present in the layered structure of the precursor during the topotactic transformation to the pyrophosphate. Stacking faults may also be used to rationalize the presence of V^{5+} sites in $(VO)_2P_2O_7$, since such faults

result in the presence of sites in which the apical oxygen of the VO_5 groups formed is unshared.

This present paper reports the results of an in situ XRD and Raman study of the evolution and crystallization of vanadyl pyrophosphate in VPO catalysts over time under catalytic reaction conditions from the crystalline $VOHPO_4 \cdot 0.5H_2O$ precursor. This study addresses: (i) the nature of the precursor transformation on the atomic, nano-, and macroscales, and (ii) the phase composition of the fresh and equilibrated catalysts under realistic catalytic reaction conditions.

2. Experimental

2.1. Synthesis

1. *Aqueous system.* The $VOHPO_4 \cdot 0.5H_2O$ precursor was prepared in aqueous medium according to a previously reported procedure [4].
2. *Organic system.* Preparation of the organic $VOHPO_4 \cdot 0.5H_2O$ precursor possessing the synthesis P/V ratio of 1.18 has been previously described [4]. The $VOHPO_4 \cdot 0.5H_2O$ precursor obtained was transformed into the catalytic $(VO)_2P_2O_7$ phase and conditioned on stream in 1.2 vol.% *n*-butane in air at 653 K for 30 days. This catalyst exhibited the selectivity to maleic anhydride of 69 mol% at 76 mol% *n*-butane conversion in 1.2 vol.% *n*-butane in air at 673 K.
3. *Model organic system.* The preparation of the model $VOHPO_4 \cdot 0.5H_2O$ precursor possessing platelet morphology has been described in detail elsewhere [4].

2.2. Characterization

2.2.1. In situ XRD

The XRD measurements were made with a Scintag PAD-X Θ – Θ X-ray diffractometer with an Anton Paar HTK-10 heating stage. Step scans were conducted using Cu $K\alpha$ radiation with a scintillation detector, and scans ranged from 10 to 80° 2Θ with a step size of 0.03° 2Θ and a count rate of 10 s per step. Powdered aqueous $VOHPO_4 \cdot 0.5H_2O$ precursors were mixed with acetone, and the suspensions were deposited as a thin layer on the heating stage, which consisted of

a Pt strip that heated in response to increased electrical current. The heating stage was enclosed within a vacuum chamber and purged with dry nitrogen gas throughout the XRD measurements to prevent the oxidation of V(IV) in $\text{VOHPO}_4 \cdot 0.5\text{H}_2\text{O}$. In the case of the $(\text{VO})_2\text{P}_2\text{O}_7$ catalyst, the heating stage was purged with 0.9 vol.% *n*-butane in air. Diffraction data were collected at room temperature (293 K) and at 583 K in the case of $\text{VOHPO}_4 \cdot 0.5\text{H}_2\text{O}$, and room temperature and 673 K in the case of $(\text{VO})_2\text{P}_2\text{O}_7$, as determined by a Pt-10% RhPt thermocouple spot-welded to the Pt strip heater. Temperature gradients across the sample area have been minimized by the attachment of a 0.254 mm thick piece of Pt foil in the center 15 mm of the strip heater to reduce the resistance of the heater in the sample area [17]. For the high temperature experiments, the sample temperature was raised to 583 and 673 K in the case of $\text{VOHPO}_4 \cdot 0.5\text{H}_2\text{O}$ and $(\text{VO})_2\text{P}_2\text{O}_7$, respectively, at a rate of 10 K/min and maintained to within ± 5 K with a Microstar 828D controller and Scintag 150 A dc power supply.

Systematic intensity errors due to angular divergence for reflections below $55^\circ 2\theta$ were corrected using empirically derived divergence function that was successfully tested with a LaB_6 standard (NIST SRM 660). In order to assess the possibility of the irreversible structural changes at high temperature, $\text{VOHPO}_4 \cdot 0.5\text{H}_2\text{O}$ specimens were heated separately in furnace at 583 K for 8 h. Comparison of powder XRD patterns from the material before and after heating revealed no discernible differences. Likewise, the similarity of the XRD patterns collected at room temperature before and after this high temperature diffraction experiment indicated no evidence for dehydration or reconstructive transformation of the $\text{VOHPO}_4 \cdot 0.5\text{H}_2\text{O}$ sample.

2.2.2. *In situ* Raman spectroscopy

The *in situ* Raman spectrometer system consisted of a quartz cell and a sample holder, a triple-grating spectrometer (Spex, Model 1877), a photodiode array detector (EG&G, Princeton Applied Research, Model 1420), and an argon ion laser (Spectra-Physics, Model 165). The sample holder was made from a metal alloy (Hastalloy C), the 100–200 mg sample disc was held by the cap of the sample holder. The sample holder was mounted onto a ceramic shaft that was rotated by a 115 V dc motor at a speed of 1000–2000 rpm. A

cylindrical heating coil surrounding the quartz cell was used to heat the sample and the temperature was measured by an internal thermocouple. The quartz cell was capable of operating up to 873 K, and flowing gas was introduced into the cell at a rate of 50–300 cm^3/min at atmospheric pressure. The 514.5 nm line of the Ar^+ laser using between 10 and 100 mW of power was focused on the sample disc in a right angle scattering geometry. An ellipsoid mirror collected and reflected the scattered light into the spectrometer's filter stage to reject the elastic scattering component. The resulting filtered light, consisting primarily of the Raman component of the scattered light, was collected with an EG&G intensified photodiode array detector which was coupled to the spectrometer and was thermoelectrically cooled to 238 K. The photodiode array detector was scanned with an EG&G OMA III optical multichannel analyzer (Model 1463).

The *in situ* Raman spectra were obtained over the 273–773 K range employing the following procedure. The $\text{VOHPO}_4 \cdot 0.5\text{H}_2\text{O}$ precursor or VPO catalyst samples were placed into the cell and the Raman spectra were collected at room temperature. The samples were then heated up to successively higher temperatures in ca. 50 K increments in either flowing pure helium or a gaseous 1:4 mixture of oxygen and 1.49% *n*-butane in helium with a flow rate of 100 cm^3/min , and the Raman spectra were collected immediately after stabilization at each set-point temperature.

2.2.3. ^{31}P spin echo NMR

The detailed description of the ^{31}P NMR experiments can be found elsewhere [4].

3. Results

3.1. $\text{VOHPO}_4 \cdot 0.5\text{H}_2\text{O}$ structure refinement

Rietveld refinement of the XRD data was accomplished using the General Structure Analysis System (GSAS) of Larson and Von Dreele [18]. Starting parameters for $\text{VOHPO}_4 \cdot 0.5\text{H}_2\text{O}$ were obtained from Leonowicz et al. [6]. Refinement for both structures was performed for values of 2θ between 20 and 80° . Five reflections produced by the Pt strip heater and a minor unidentified peak with $d_{hkl} = 2.12 \text{ \AA}$ were excluded from the analysis. The following parameters

Table 1
Refinement data for VOHPO₄·0.5H₂O structure at room temperature and 583 K

	Temperature		
	Room temperature ^a	293 K ^b	583 K ^b
Space Group	<i>Pmmn</i>	<i>Pmmn</i>	<i>Pmmn</i>
<i>a</i> (Å)	7.420(1)	7.4223(6)	7.4509(6)
<i>b</i> (Å)	9.609(2)	9.6109(8)	9.6058(7)
<i>c</i> (Å)	5.6931(7)	5.6993(3)	5.7371(3)
Volume (Å ³)	405.9(4)	406.55(2)	410.62(6)
Density (g/cm ³)	2.81	2.792	2.765
exp <i>R</i> _w	0.041	0.0679	0.0794
<i>R</i> _{wp}	0.042	0.0968	0.1138
Reduced χ^2		2.035	2.099

^a Leonowicz et al. [6].

^b This work.

were refined: (i) scale factor; (ii) specimen displacement; (iii) background, which was modeled by 18 refinable coefficients in a cosine Fourier series; (iv) lattice parameters; (v) preferred orientation parallel to (00 1) to account for the strong basal cleavage exhibited by the material; (vi) profile shapes, which were fitted to symmetric pseudo-Voigt functions (previous refinement of a LaB₆ standard (NIST SRM 660) provided starting values for the profile parameters, Gaussian Caglioti coefficients were held constant, and only the Lorentzian components and the Scherrer coefficient for Gaussian broadening were varied); and (vii) fractional coordinates for V, P, and O. In both experiments, the P(1)–O(1) distance refined to unreasonably high values (ca. 1.64 Å), presumably as a result of O(1)–H(2) bonding. Consequently, the P(1)–O(1) bond was fixed at 1.56 Å by soft constraint. Upon convergence, the goodness of fit as measured by χ^2 was 2.035 and 2.099 for the room temperature and the 583 K analyses. Refinement results are presented in Table 1, and refined fractional coordinates are included in Table 2.

Refinement of the room temperature structure of VOHPO₄·0.5H₂O from powder XRD data was in strong agreement with the single crystal results presented by Torardi and Calabrese [5] and Leonowicz et al. [6]. The structure consists of face-sharing VO₆ octahedra that are corner-linked by phosphate tetrahedra to form sheets parallel to (00 1) (Fig. 1). Within each VO₆ octahedron, a single V–O(4) double bond is indicated by a refined bond length of ca. 1.56 Å.

Table 2
Fractional coordinates for VOHPO₄·0.5H₂O structure at room temperature and 583 K (origin at –1)

Atom	Temperature (K)	<i>x</i>	<i>y</i>	<i>z</i>
V(1)	293	0.0431(6)	0.25	0.0322(5)
	583	0.0440(6)	0.25	0.0334(5)
P(1)	293	0.25	0.5327(7)	0.2144(8)
	583	0.25	0.5316(7)	0.2078(8)
O(1)	293	0.25	0.5137(17)	0.4879(9)
	583	0.25	0.5082(15)	0.4777(9)
O(2)	293	0.0830(13)	0.6084(10)	0.1521(13)
	583	0.0834(12)	0.6056(10)	0.1499(12)
O(3)	293	0.25	0.3889(15)	0.1133(19)
	583	0.25	0.3855(15)	0.1123(17)
O(4)	293	–0.0623(19)	0.25	0.2768(15)
	583	–0.0502(20)	0.25	0.2753(18)
O(5)	293	0.25	0.25	–0.2852(21)
	583	0.25	0.25	–0.2844(25)
H(1) ^a	293	0.25	0.178	0.629
	583	0.25	0.178	0.629

^a Position determined from observed Fourier synthesis maps.

The two previous studies of VOHPO₄·0.5H₂O discerned positional disorder for O(1) and O(4). The powder diffraction data in this study did not support a determination of anisotropic temperature coefficients, but observed Fourier synthesis maps do reveal an anisotropic electron density distribution for these atoms parallel to (1 0 0) and [0 1 0], respectively. In addition, O(5) displayed elongated electron density contours parallel to (1 0 0) and perpendicular to the H(1)–O(5)–H(1) plane. As noted in the earlier studies [5,6], these slight displacements from mirror planes suggest that the oxygen atoms are either statically or dynamically disordered between proximal sites.

Neighboring layers in VOHPO₄·0.5H₂O are hydrogen-bonded via molecular water groups and hydroxyl groups. This structural hydrogen accounts for the refined V–O(5) length of 2.37 Å, which is unusually long due to two H(1) atoms bonded to O(5). Leonowicz et al. [6] identified, but did not refine the position of H(1) at (0.25, 0.166, 0.668). This location results in reasonable H–O bond distances, but the H(1)–O(5)–H(1) bond angle is nearly 140°, somewhat removed from the ideal tetrahedral angle of 109.5°. Examination of observed Fourier maps in

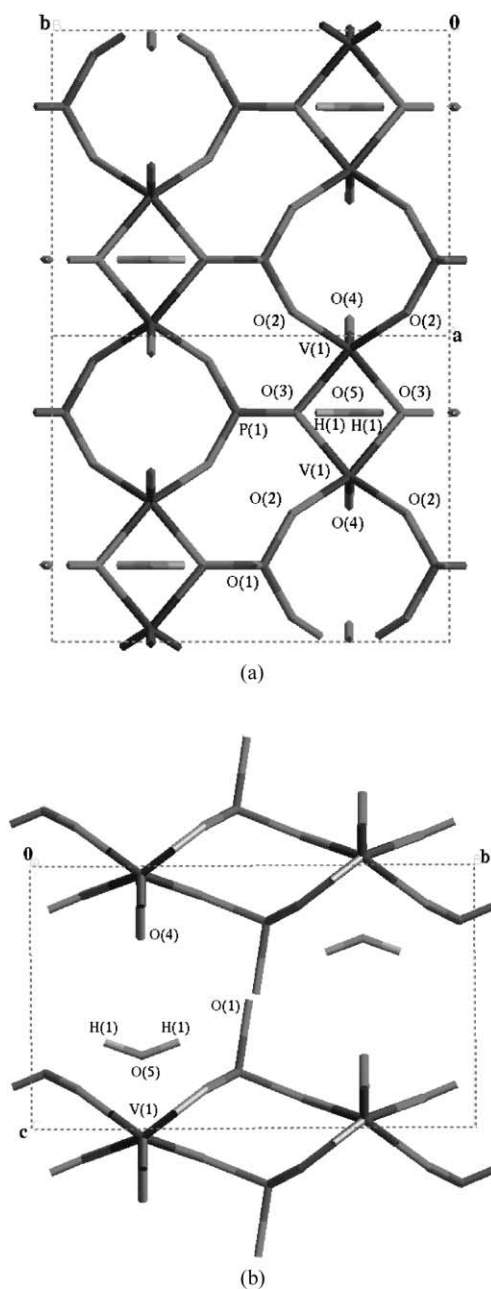


Fig. 1. Projections of the structure of $\text{VOHPO}_4 \cdot 0.5\text{H}_2\text{O}$ (a) along the $[001]$ axis; and (b) off the (100) axis.

the present study suggests a slightly different position for H(1) at (0.25, 0.178, and 0.629). Relocation of H(1) to this position lowered the value of χ^2 by 0.05 in both refinements, and it produces an H–O–H

bond angle close to tetrahedral geometry. In addition, it maintains a hydrogen-bonded $\text{O}(1)\text{--H}(1)\cdots\text{O}(5)$ angle near 170° . As with the earlier studies [5,6], the location of H(2) could not be determined, though the refined bond length of 1.65 \AA for $\text{P}(1)\text{--O}(1)$ supports the speculation of Leonowicz et al. [6] that H(2) is bonded to O(1) to form a hydrogen bond with O(4).

Heating $\text{VOHPO}_4 \cdot 0.5\text{H}_2\text{O}$ to 583 K resulted in only subtle changes in the structure and yielded no evidence for a symmetry-changing phase transition. The unit cell volume increased by 1.00% with the temperature increase of 290 K. This overall expansion resulted from increases in the lengths of a and c , as b contracted with higher temperature. Thus, minor extension occurred parallel to the $(\text{VO}_6)_2$ chains and along the hydrogen-bonded layers. Both the PO_4 and the VO_6 polyhedra remained quite rigid with increase in temperature. At 293 K $\langle\text{P--O}\rangle_{\text{ave}} = 1.50 \pm 0.04 \text{ \AA}$ and $\langle\text{V--O}\rangle_{\text{ave}} = 2.01 \pm 0.25 \text{ \AA}$, and the values at 583 K are different only in terms of standard deviation, with $\langle\text{P--O}\rangle_{\text{ave}} = 1.50 \pm 0.05 \text{ \AA}$ and $\langle\text{V--O}\rangle_{\text{ave}} = 2.01 \pm 0.27 \text{ \AA}$. The observed rigidity of the PO_4 tetrahedra is consistent with high temperature studies of other phosphates, such as the AlPO_4 polymorph berlinite [19].

Torardi and Calabresi [5] argued that below ca. 143 K the oxygen atoms in $\text{VOHPO}_4 \cdot 0.5\text{H}_2\text{O}$ invert from positional disorder to an ordered arrangement, which induces a doubled periodicity along c . Examination of the elongated electron density contours for O(1), O(4), and O(5) in the present study at 583 K revealed no change in eccentricity from room temperature. If the positional disorder is dynamic, rather than static, the increase in temperature apparently does not increase the amplitude of the oscillation. Moreover, Fourier observed maps revealed the presence of H(1) atoms bonded to O(5) at 583 K at close to the room temperature position. This observation and the insignificant change in the magnitude of the basal spacing suggest that little or no dehydration occurred during the course of these experiments.

3.1.1. Thermal transformation of $\text{VOHPO}_4 \cdot 0.5\text{H}_2\text{O}$

The in situ Raman spectra of the model organic $\text{VOHPO}_4 \cdot 0.5\text{H}_2\text{O}$ precursor during its thermal transformation in inert helium atmosphere at 298–823 K are shown in Fig. 2a. Thermal broadening and gradual loss of long and short range order in $\text{VOHPO}_4 \cdot$

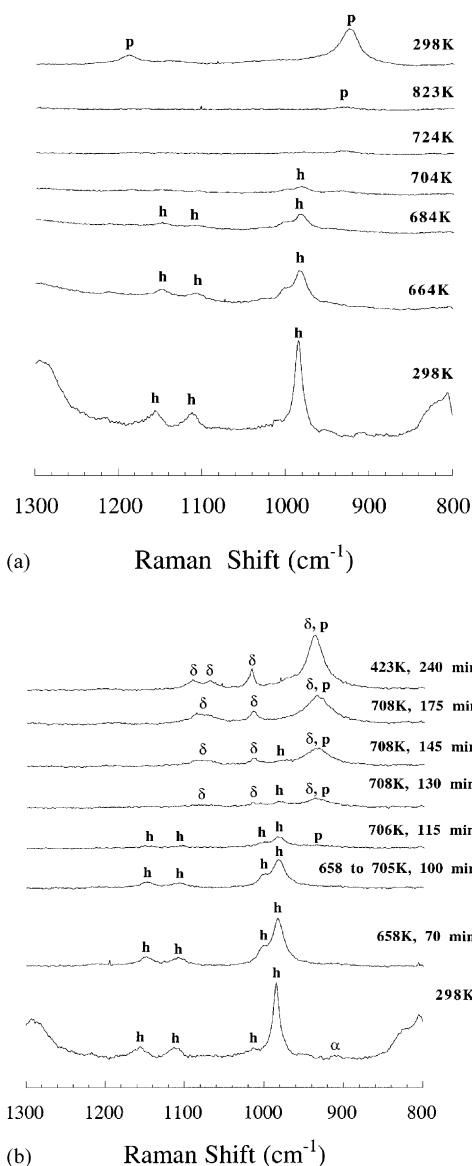


Fig. 2. In situ Raman spectra of $\text{VOHPO}_4 \cdot 0.5\text{H}_2\text{O}$ at (a) 298–823 K in flowing He at $100\text{ cm}^3/\text{min}$; and (b) 298–708 K in flowing 1:4 mixture of oxygen and 1.49 mol% *n*-butane in He at $100\text{ cm}^3/\text{min}$.

$0.5\text{H}_2\text{O}$ is observed in the in situ Raman spectra as $\text{VOHPO}_4 \cdot 0.5\text{H}_2\text{O}$ is heated to 704 K. The characteristic P–O stretch of $\text{VOHPO}_4 \cdot 0.5\text{H}_2\text{O}$ observed at 981 cm^{-1} was shifted slightly to 979 cm^{-1} at 684–704 K; a new shoulder at 1002 cm^{-1} is also

observed at elevated temperatures. Above 704 K, even the local order is lost and after further heating to 823 K, the weak P–O stretch of the poorly crystalline vanadyl pyrophosphate is observed in the in situ Raman spectra at ca. 930 cm^{-1} . Nevertheless, no other crystalline phase was observed for the in situ Raman spectra at 823 K, even after cooling to room temperature.

Similar loss of crystallinity was observed during the $\text{VOHPO}_4 \cdot 0.5\text{H}_2\text{O}$ transformation in the reactive *n*-butane and oxygen-containing atmosphere (Fig. 2b). However, in this case vanadyl(IV) pyrophosphate and oxidized $\delta\text{-VOPO}_4$ are already observed along with $\text{VOHPO}_4 \cdot 0.5\text{H}_2\text{O}$ at 708 K, in agreement with previous observations [21]. The transformation of $\text{VOHPO}_4 \cdot 0.5\text{H}_2\text{O}$ into a mixture of vanadyl(IV) pyrophosphate and $\delta\text{-VOPO}_4$ is complete at 708 K within 45 min. In a previous study [4], the Raman scattering cross-section of $\delta\text{-VOPO}_4$ was found to be approximately three times that of vanadyl(IV) pyrophosphate. Therefore, even a minor $\delta\text{-VOPO}_4$ component present in slightly oxidized fresh catalysts may be detected using Raman spectroscopy (Fig. 2b).

3.1.2. Equilibrated VPO catalysts under reaction conditions

The changes in the equilibrated organic VPO catalysts as a function of temperature in the reactive *n*-butane and oxygen-containing atmosphere were followed by the in situ XRD and Raman techniques. Prior to the in situ experiments, these catalysts were equilibrated for over 30 days using 1.2 vol.% *n*-butane in air at 653 K. The in situ XRD patterns and Raman spectra are shown in Figs. 3 and 4, respectively. Both of these experimental techniques demonstrated that the equilibrated VPO catalysts contained only crystalline vanadyl pyrophosphate under catalytic reaction conditions studied. The intensity of the asymmetric pyrophosphate P–O stretch observed at 921 cm^{-1} decreased at high temperature as the result of thermal broadening and its position shifted to higher wavenumbers, 929.5 cm^{-1} (Fig. 4). The room temperature ^{31}P spin echo NMR spectrum of the equilibrated organic catalyst (Fig. 5) showed a single peak at ca. 2400 ppm characteristic of vanadyl pyrophosphate and no minor diamagnetic VOPO_4 phases expected at ca. 0 ppm [4].

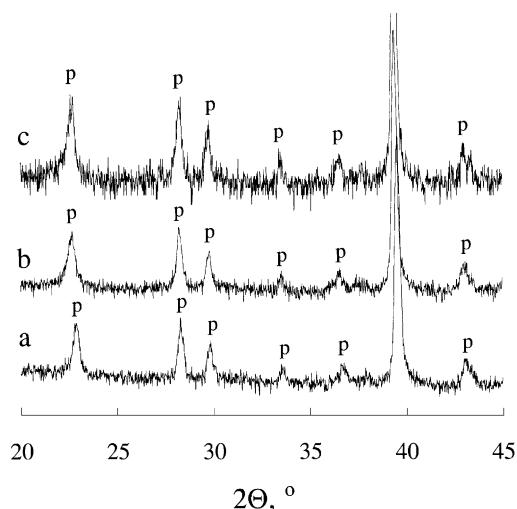


Fig. 3. In situ XRD patterns of the equilibrated organic VPO catalyst at (a) room temperature; (b) 653 K; and (c) in flowing 0.9 mol% *n*-butane in air at 30 cm³/min and 653 K.

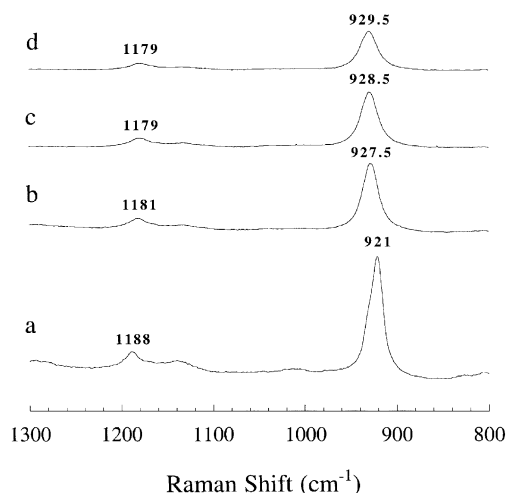


Fig. 4. In situ Raman spectra of the equilibrated organic VPO catalyst in flowing 1:4 mixture of oxygen and 1.49 mol% *n*-butane in He at 100 cm³/min at (a) 298; (b) 533; (c) 618; and (d) 653 K.

4. Discussion

4.1. Atomic scale changes in VOHPO₄·0.5H₂O structure at high temperature

The high temperature structure of VOHPO₄·0.5H₂O shows no evidence of the loss of the structural water.

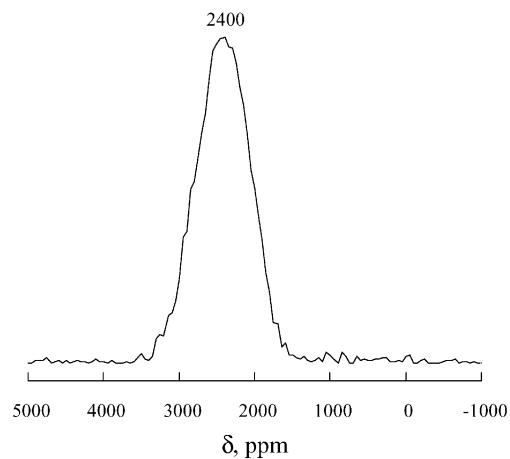


Fig. 5. ³¹P spin echo NMR spectrum of the equilibrated organic VPO catalyst at room temperature.

The *d*-spacing increases slightly with temperature from 5.699 to 5.737 Å, which may indicate slight weakening of the interlayer hydrogen bonding. In fact, the V–OH₂ distance between the oxygen atom of the structural water molecule and the vanadium atom to which it is coordinated increases slightly with temperature from 2.373 to 2.383 Å. At the same time, the hydrogen bond between the protons of the structural water and the oxygens of the P–OH groups in the adjacent layers shortens from 2.010 to 1.988 Å. These observations may be interpreted as the early manifestation of the thermal transformation. Thus, the *d*-spacing increases with temperature due to thermal expansion leading to weakened H-bonding between the layers (Fig. 1b), while structural water molecules leave the coordination sphere of the *cis*-vanadyl dimers to hydrogen-bond with the P–OH groups prior to their loss in dehydration. Simultaneously, we may postulate that the V=O groups begin to rotate to a parallel arrangement relative to each other in a *cis*-vanadyl dimer, observed in a decrease of the angle between the V=O bond and the *c*-axis from 29.35 to 26.80° with temperature. In this manner, the distance between the equatorial oxygens in a *cis*-vanadyl dimer along the shared face (Fig. 1a) contracts from 2.670 to 2.603 Å with increase in temperature. This is the same distance which is observed in the vanadyl(IV) pyrophosphate structure at room temperature. The V–V distance in the vanadyl dimer does not change with temperature (3.070 Å) and is much shorter than the

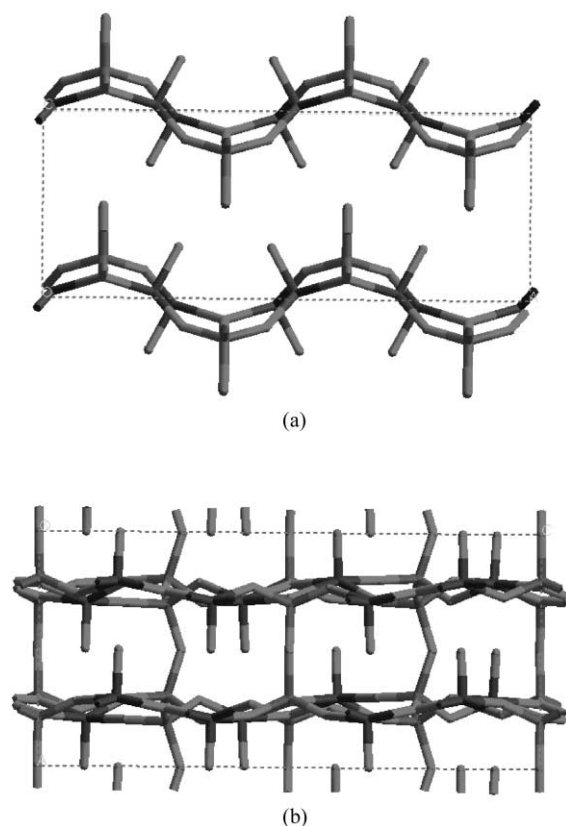


Fig. 6. Projections of the structure of (a) $\text{VOHPO}_4 \cdot 0.5\text{H}_2\text{O}$ onto the ac plane; and (b) $(\text{VO})_2\text{P}_2\text{O}_7$ onto the bc plane.

corresponding distance in the vanadyl(IV) pyrophosphate at room temperature, 3.231 \AA [8]. A slight expansion of the a -axis is also observed (Fig. 1a). Since the V–V distance in the dimer does not change with temperature, the a -axis expansion occurs at the expense of flattening of the layers. In fact, the a -axis expansion due to the increase in the V–V distance would only contribute 0.32 \AA per unit cell or 4.3% of the a -parameter and should result in $c/2 = 7.7423 \text{ \AA}$ in vanadyl pyrophosphate. However, the $c/2$ axis in vanadyl pyrophosphate is 8.29425 \AA , and the additional increase of 0.55195 \AA or 7.4% per unit cell may be assumed to be due to the flattening of the undulating HPO_4 layers in the precursor phase during the thermal transformation (see Fig. 6). The distance between the phosphate tetrahedra along the b -axis increases with temperature (4.196 \AA at 583 K versus 4.177 \AA at 293 K) resulting in a shorter structural

$\text{H}_2\text{O} \dots \text{O}(\text{H})\text{P}$ hydrogen bond distance. These observations are further examined in the light of two recent structural transformation models [11,12].

The recently proposed models of the $\text{VOHPO}_4 \cdot 0.5\text{H}_2\text{O}$ transformation into $(\text{VO})_2\text{P}_2\text{O}_7$ [11,12] are based on the observed similarities between the single crystal structures of these phases. According to Amorós et al. [12], the dehydration process begins with concerted displacement of the basal layers of $\text{VOHPO}_4 \cdot 0.5\text{H}_2\text{O}$ along the $[110]$ direction to align the HPO_4^{2-} groups on the adjacent layers for condensation into $\text{P}_2\text{O}_7^{4-}$ groups. The elimination of the structural water and the condensation of the layers are also concerted processes. The total synchronism of this displacement could be easily disrupted by local defects leading to a disordered intermediate, requiring high temperatures for complete conversion into crystalline $(\text{VO})_2\text{P}_2\text{O}_7$ [12]. Amorós et al. detected the disordered intermediate after elimination of ca. 60% of water obtained from the hydrogen phosphate groups. However, such concerted displacement of the layers relative to one another should also result in disruption of orthorhombic symmetry in $\text{VOHPO}_4 \cdot 0.5\text{H}_2\text{O}$, which was not observed in the present study.

Conversely, Torardi et al. [11] proposed a phosphorus inversion model, which provided a detailed explanation for the formation of the P–O–P connectivity without the orthorhombic symmetry change during the transformation. Therefore, the changes observed in the precursor structure at high temperature in the present study are further discussed in terms of the phosphorus inversion model.

According to the phosphorus inversion model proposed by Torardi et al., the structural water coordinated to the vanadyl dimers is lost first, followed by a decrease in the interlayer spacing. Next, the VO_5 groups pivot about the shared edge in each vanadyl dimer to an arrangement where all V=O bonds are approximately parallel, leading to the 12% increase in the a -lattice parameter. Subsequently, the protons from half of the HPO_4^{2-} groups transfer to the remainder of the HPO_4^{2-} groups to yield the PO_4^{3-} and $\text{H}_2\text{O}-\text{PO}_3^-$ units. Removal of further water from these latter units ($\text{H}_2\text{O}-\text{PO}_3^- \rightarrow \text{PO}_3^- + \text{H}_2\text{O}$) allows the layers to fully condense into the pyrophosphate structure. Half of the vanadyl oxygens displace in the c direction to produce edge-sharing *trans*-vanadyl dimers. Ultimately, the coordinatively unsaturated

PO_3^- groups invert through a plane of the three basal oxygen atoms to bond to PO_4^{3-} units located above or below the original layer. The resulting vanadyl pyrophosphate structure is expected to display a disorder in the arrangement of the pyrophosphate groups that hold the layers together. Much higher temperatures or longer times under catalytic reaction conditions are required to break and reform the P–O–P bonds into the observed ordered 3D arrangement [7–10]. While the model of Torardi et al. does not require the complete loss of the crystalline order, some disorder in the pyrophosphate groups and vanadium atoms along the *c*-axis is expected [9,20].

However, these proposed HPO_4^{2-} dehydration and phosphorus inversion steps [11] may require a high energy of activation, since they involve the generation and subsequent condensation of a large number of PO_3^- and PO_4^{3-} groups, which bear locally uncompensated charges of the same sign, to form the P–O–P bonds. Conversely, the dehydration of the HPO_4^{2-} layers into $(\text{VO})_2\text{P}_2\text{O}_7$ may occur via a nucleophilic attack of the oxygen attached to the de-protonated $\text{O}_3\text{P}-\text{O}^{3-}$ groups in one layer on the phosphorus atom in the di-protonated PO_3OH_2^- moieties in the layer above. For this reaction, proceeding via inversion of the PO_3^- tetrahedron to form a P–O–P linkage, the water molecule is a good leaving group. If we consider the hydrogen bonding scheme suggested by Leonowicz et al., for the room temperature structure of $\text{VOHPO}_4 \cdot 0.5\text{H}_2\text{O}$, the proton transfer between the HPO_4^{2-} groups that precedes the condensation may be mediated by the vanadyl oxygens shown in Fig. 4 [6]: $\text{V(IV)}=\text{O}_2^+ + \text{H}-\text{OPO}_3^{2-} \rightarrow \text{V(IV)}-\text{OH}_3^+ + \text{OPO}_3^{3-}$. This proton transfer is likely to decrease the V=O bond order, elongate this bond along the *b*-axis and bring the vanadyl O atom closer to the V atom in the layer above, thereby promoting the conversion of *cis*-vanadyl dimers to the *trans* arrangement observed in $(\text{VO})_2\text{P}_2\text{O}_7$. Thus, the OH group would migrate to the V atom directly in the adjacent layer followed by a proton transfer back to a neighboring PO_4^{3-} or HPO_4^{2-} group, resulting in the *trans*-vanadyl oxygen arrangement. This scheme suggests both the mechanism of the proton transfer as well as the role of protons as catalysts in the *cis/trans* transformation step. The complete condensation into the reported pyrophosphate structure [7–10] requires a perfectly ordered alignment of the

phosphate groups. However, proton transfer between the HPO_4^{2-} groups may occur randomly and result in an incomplete condensation of all HPO_4^{2-} groups into the pyrophosphate network. Assuming a random distribution of half of the protons, any particular PO_4^{3-} or PO_3OH_2^- group has 50% probability of finding a complementary group in the adjacent layer suitable for initial condensation into the P–O–P linkages. Assuming irreversibility of the P–O–P bond formation at low temperatures, there is 75% probability that any particular phosphate group would eventually form a P–O–P bond due to further proton diffusion according to $2\text{HPO}_4^{2-} \rightarrow \text{PO}_4^{3-} + \text{PO}_3\text{OH}_2^-$. Such partially transformed intermediate would be characterized by a significant variation of the local order and the *d*-spacing leading to its disordered character on the nanoscale in agreement with the earlier observations made by Amorós et al. [12]. It should be noted that Amorós et al. [12] observed that the disordered intermediate was formed after evolution of ca. 60% water from the condensation reaction of the HPO_4^{2-} groups. If one also accounts for the loss of the surface-adsorbed moisture, the observed weight loss (ca. 60%) is indeed close to the 50% mark, corresponding to random distribution of the PO_4^{3-} or PO_3OH_2^- groups on the adjacent layers. This observation may indicate that the initial condensation step leading to the disordered intermediate occurs faster than the accompanying redistribution of the protons, which would result in the evolution of 75% of water due to such condensation reactions. Such disordered pyrophosphate structure may contain ca. 25% of the isolated HPO_4^{2-} groups, which were unable to form pyrophosphate linkages. At higher temperatures, poorly crystalline $(\text{VO})_2\text{P}_2\text{O}_7$ would be formed due to further proton diffusion, rearrangement and condensation of the residual HPO_4^{2-} groups present on the phosphate layers. The fully ordered $(\text{VO})_2\text{P}_2\text{O}_7$ structure is observed only at higher (near melt) temperatures after a complete dehydration of the HPO_4^{2-} groups and the P–O–P bond breaking and reformation [7–10].

The results of the present high temperature XRD study do not provide insights into the further steps of dehydration and condensation into the vanadyl(IV) pyrophosphate structure. Further changes in the nanoscale order of the precursor were studied by the in situ Raman spectroscopy.

4.2. Evolution of nano- and macroscale order during VOHPO₄·0.5H₂O transformation

In agreement with the earlier findings [12], gradual loss of the nanoscale order in VOHPO₄·0.5H₂O was observed as the model organic VOHPO₄·0.5H₂O precursor was heated from 583 to 704 K under He atmosphere (Fig. 2a). Above this temperature the structure was completely disordered and nanocrystalline vanadyl pyrophosphate (ca. 10 nm domains by XRD) was observed for the in situ Raman spectra only at 823 K, in agreement with the transformation mechanism proposed above. The precursor and the pyrophosphate phase did not coexist under these dehydration conditions in agreement with the previous observations of Amorós et al. [12] and Volta coworkers [21,22]. Furthermore, Amorós et al. [12] observed the transformation of the higher hydrates of VOHPO₄·*n*H₂O (*n* = 1–4) to (VO)₂P₂O₇ in a powder neutron diffraction study. Remarkably, all crystalline hydrates, including VOHPO₄·0.5H₂O, coexisted with one another during the sequential dehydration. However, it was observed that the solid-state transformation of VOHPO₄·0.5H₂O into (VO)₂P₂O₇ proceeded via a disordered intermediate [12,21]. It is interesting that the structures and the V–O–P connectivity of the higher hydrates are very different from those of VOHPO₄·0.5H₂O. They contain isolated vanadyl octahedra, which transform to the face-sharing vanadyl dimer coordination in VOHPO₄·0.5H₂O upon dehydration. Given the much closer similarity between these two structures, it is remarkable that the crystalline hemihydrate and pyrophosphate structures were not observed to coexist during the dehydration experiments of Amorós et al. [12]. However, when this transformation was conducted in the reactive *n*-butane and oxygen-containing atmosphere, vanadyl(IV) pyrophosphate and oxidized δ-VOPO₄ were readily observed along with VOHPO₄·0.5H₂O at 708 K with in situ Raman (Fig. 2b).

Volta and coworkers [21,22] also observed formation of oxidized α_{II}-, δ- and γ-VOPO₄ phases during the activation of the VOHPO₄·0.5H₂O precursor in the *n*-butane/air atmosphere by in situ Raman spectroscopy. They considered two parallel routes for the transformation of the precursor: (i) oxidehydration of VOHPO₄·0.5H₂O to VOPO₄ phases, accompanied by a slow reduction of δ-VOPO₄ to (VO)₂P₂O₇ and

transformation to α_{II}-VOPO₄; and (ii) the dehydration of VOHPO₄·0.5H₂O to (VO)₂P₂O₇ [22]. However, it seems most likely that the appearance of the oxidized phases in these cases is probably caused by the poor heat and mass transfer conditions during in situ Raman experiments.

The considerable differences between the ex situ and in situ catalysts during the activation, and the presence of VOPO₄ phases at the moment of the transformation of the precursor, were also observed by Overbeek et al. [23] using X-ray diffraction. They observed that the VPO catalysts were a mixture of unknown VOPO₄ phases under catalytic reaction conditions and contained only (VO)₂P₂O₇ after exposure to air at room temperature. However, formation of crystalline VOPO₄ phases detected by XRD typically occurred under even stronger oxidizing conditions than those employed in the in situ Raman studies [4]. Transformation of (VO)₂P₂O₇ [24,25] and various VOPO₄ phases [25] into a “new, slightly anion-deficient phase” [24] and V₂O₅ [25] during their exposure to water vapor at high temperatures has been recently reported. Xue and Schrader [25] observed transformation of (VO)₂P₂O₇ into V₂O₅ by in situ Raman after the VPO catalyst was exposed to 5–10% water vapor at 723 K. Formation of the surface V₂O₅ phase was reversible after a short-term exposure to water vapor, and the surface phosphate lost due to hydrolysis was probably replenished by diffusion of the phosphate anions from the crystalline bulk. After a prolonged exposure to water vapor and a significant phosphate loss, the bulk V₂O₅ phase formed irreversibly.

These previous observations [21–25] further emphasized the extreme sensitivity of the VPO catalysts to various reducing, oxidizing and hydrolytic environments. However, when the typical dry 1.2 vol.% *n*-butane/air feed was used, the VOHPO₄·0.5H₂O precursor transformed inside a catalytic microreactor contained only vanadyl pyrophosphate and no other nanocrystalline VPO or V₂O₅ phase [26].

Evolution of the nanocrystalline vanadyl pyrophosphate and other oxidized VOPO₄ phases coincided with an onset of *n*-butane oxidation activity and selectivity of the VPO catalysts [21,22]. However, the selectivity of these fresh catalysts to maleic anhydride was low (e.g. 30–45 mol%) as compared with the equilibrated catalysts (e.g. 70–80 mol%) and improved over

time during on-stream conditioning [3,8,21,22,26]. During this conditioning procedure, the disordered $(\text{VO})_2\text{P}_2\text{O}_7$ phase gradually crystallized in the bulk VPO catalysts over a period of hundreds of hours.

High-resolution TEM studies detected a disordered layer ca. 2 nm thick covering the surface (100) planes of $(\text{VO})_2\text{P}_2\text{O}_7$ in fresh catalysts [26]. This nanoscale structural feature became progressively less pronounced with time on stream, and could be no longer detected by TEM after a few weeks under catalytic reaction conditions. It was concluded that a specific surface termination of the (100) planes of $(\text{VO})_2\text{P}_2\text{O}_7$ was responsible for a significant improvement of selectivity to maleic anhydride for the equilibrated catalysts [26].

The phase analysis of the equilibrated VPO catalysts is typically conducted ex situ under very different conditions, i.e. in the absence of the catalytic reaction. The phase composition of the equilibrated organic VPO catalyst under catalytic reaction conditions was studied here employing in situ XRD and Raman methods (Figs. 3 and 4). This catalyst was conditioned in flowing 1.2 vol.% *n*-butane in air at 653 K for 30 days. The in situ XRD and Raman methods and ambient ^{31}P spin echo NMR (Fig. 5) indicated that the equilibrated VPO catalysts contained only $(\text{VO})_2\text{P}_2\text{O}_7$ (ca. 30 nm domains) under both the ambient and *n*-butane oxidation conditions, although the intensity of the XRD and Raman signal decreased at high temperature due to increased thermal broadening. In addition to thermal broadening, the asymmetric P–O pyrophosphate stretch observed at 921 cm^{-1} at ambient temperature shifted to higher frequency, 929.5 cm^{-1} , at 653 K (Fig. 4). High temperature X-ray structural studies of single crystal $(\text{VO})_2\text{P}_2\text{O}_7$ may provide new insights into the pyrophosphate anion geometry and the origin of this shift. The previous observations of minor phases other than $(\text{VO})_2\text{P}_2\text{O}_7$ under catalytic reaction conditions may be explained by a reversible oxidation of $(\text{VO})_2\text{P}_2\text{O}_7$ in the VPO catalysts at high temperature and *n*-butane lean oxidizing conditions into nanocrystalline δ - and γ -VOPO₄ phases [25,27,28]. The best $(\text{VO})_2\text{P}_2\text{O}_7$ catalysts were stable under the typical fixed bed conditions (1.2–1.5 vol.% *n*-butane in air at a GHSV of 1000–2000 h⁻¹ and 653–713 K) and did not form nanocrystalline oxidized phases.

5. Conclusion

In the present paper, the transformation of the catalytic VOHPO₄·0.5H₂O precursor to well-crystallized $(\text{VO})_2\text{P}_2\text{O}_7$ in the equilibrated VPO catalysts was studied over several length scales by in situ and ex situ Raman and XRD techniques. The refinement of the room temperature structure of VOHPO₄·0.5H₂O resulted in an improved location of the structural water molecule coordinated to the edge-sharing vanadyl(IV) dimers. The structure of the VOHPO₄·0.5H₂O precursor was stable up to 583 K in dry nitrogen during in situ XRD experiments.

Minor atomic scale changes in the precursor structure observed at 583 K, such as the rotation of the V=O moieties, weakening of the hydrogen bonding, migration of the structural water molecules during dehydration, and flattening of the HPO₄ layers, were indicative of the early stages of the precursor transformation and consistent with the phosphorus inversion model of transformation. Furthermore, the random nature of the proton transfer between the HPO₄²⁻ groups was suggested to be responsible for the incomplete condensation of these groups in the fresh catalysts under typical catalytic reaction conditions and the formation of the disordered intermediate. The HPO₄²⁻ protons were also indicated as the catalytic species in the *cis*- to *trans*-vanadyl conversion step. Complete transformation to well-crystalline $(\text{VO})_2\text{P}_2\text{O}_7$ gradually occurred under catalytic reaction conditions via the breakup and rearrangement of the P–O–P connectivity.

Nanocrystalline oxidized VOPO₄ phases were detected by in situ Raman spectroscopy when the precursor was transformed in the reactive *n*-butane/air atmosphere in agreement with earlier observations, possibly due to the specificity of the in situ conditions. However, the precursors transformed under typical plug flow conditions in the *n*-butane/air atmosphere contained only poorly crystalline $(\text{VO})_2\text{P}_2\text{O}_7$ and no nanocrystalline oxidized phases.

Freshly transformed VPO catalysts were characterized by low activity in *n*-butane oxidation and selectivity to maleic anhydride. Nanocrystalline $(\text{VO})_2\text{P}_2\text{O}_7$ and the disordered component present in the fresh catalysts gradually transformed into well-crystalline $(\text{VO})_2\text{P}_2\text{O}_7$ in equilibrated VPO catalysts over a period of hundreds of hours under catalytic reaction conditions.

Both the in situ XRD and Raman techniques indicated that the equilibrated bulk VPO catalysts contained only crystalline $(VO)_2P_2O_7$ under catalytic reaction conditions. The conditioning process increased the surface area of the catalysts and resulted in a specific surface termination of the (1 0 0) planes of $(VO)_2P_2O_7$ in the equilibrated VPO catalysts, a phase believed to be responsible for high steady-state activity and selectivity of these catalysts in partial oxidation of *n*-butane.

Acknowledgements

This work was supported by the Grants from the University of Cincinnati Research and Faculty Development Councils, BP AMOCO Corporation (Princeton), and National Science Foundation CTS-9417981 (Lehigh).

References

- [1] F. Cavani, F. Trifiró, *Catal.* 11 (1976) 246.
- [2] G.J. Hutchings, C.J. Kiely, M.T. Sananes-Schulz, A. Burrows, J.-C. Volta, *Catal. Today* 40 (1998) 273.
- [3] S. Albonetti, F. Cavani, F. Trifiró, P. Venturoli, G. Calestani, M. Lopéz Granados, J.L.G. Fierro, *J. Catal.* 160 (1996) 52.
- [4] V.V. Guliants, J.B. Benziger, S. Sundaresan, I.E. Wachs, J.-M. Jehng, J.E. Roberts, *Catal. Today* 28 (1996) 275.
- [5] C.C. Torardi, J.C. Calabrese, *Inorg. Chem.* 23 (1984) 1310.
- [6] M.E. Leonowicz, J.W. Johnson, J.F. Brody, H.F. Shannon, J.M. Newsam, *J. Solid State Chem.* 56 (1985) 370.
- [7] N.E. Middlemis, Ph.D. Thesis, McMaster University, Hamilton, Ont., Canada, 1978.
- [8] S. Linde, L. Gorbunova, *Dokl. Akad. Nauk SSSR* 245 (1979) 584.
- [9] J.R. Ebner, M.R. Thompson, in: R.K. Grasselli, A.W. Sleight (Eds.), *Structure-Activity and Selectivity Relationships in Heterogeneous Catalysis*, Elsevier, Amsterdam, 1991, p. 31.
- [10] P.T. Nguyen, R.D. Hoffman, A.W. Sleight, *Mater. Res. Bull.* 30 (1995) 1055.
- [11] C.C. Torardi, Z.G. Li, H.S. Horowitz, W. Liang, M.-H. Whangbo, *J. Solid State Chem.* 119 (1995) 349.
- [12] P. Amorós, R. Ibáñez, A. Beltrán, D. Beltrán, A. Fuertes, P. Gomez-Romero, E. Hernandez, J. Rodriguez-Carvajal, *Chem. Mater.* 3 (1991) 407.
- [13] J.W. Johnson, D.C. Johnston, A.J. Jacobson, J.F. Brody, *J. Am. Chem. Soc.* 106 (1984) 8123.
- [14] E. Bordes, P. Courtine, J.W. Johnson, *J. Solid State Chem.* 55 (1984) 270.
- [15] Z. Hiroi, M. Azuma, Y. Fujishiro, T. Saito, M. Takano, F. Izumi, T. Kamiyama, T. Ikeda, *J. Solid State Chem.* 146 (1999) 369.
- [16] P.T. Nguyen, A.W. Sleight, N. Roberts, W.M. Warren, *J. Solid State Chem.* 122 (1996) 259.
- [17] N.E. Brown, S.M. Swapp, C.L. Bennett, A. Navrotsky, *J. Appl. Cryst.* 26 (1993) 77.
- [18] A.C. Larson, R.B. Von Dreele, *Generalized Structure Analysis System (GSAS)*: Los Alamos National Laboratory Report LAUR 86-748, 1994.
- [19] H.N. Ng, C. Calvo, *J. Phys. C* 17 (1976) 1375.
- [20] J.R. Ebner, M.R. Thompson, *Catal. Today* 16 (1993) 51.
- [21] G.J. Hutchings, A. Desmartin-Chomel, R. Olier, J.-C. Volta, *Nature* 368 (1994) 41.
- [22] J.-C. Volta, *Catal. Today* 32 (1996) 29.
- [23] R.A. Overbeek, M. Verslujs-Helder, P.A. Warringa, E.J. Bosma, J.W. Geus, in: S.V., Bellon, V.C. Corberan (Eds.), *New Developments in Selective Oxidation*, Benalmadena, Spain, *Stud. Surf. Sci. Catal.* 84 (1994) 183.
- [24] P.L. Gai, K. Kourtakis, G.W. Coulston, G.C. Sonnichsen, *J. Phys. Chem. B* 101 (1997) 9916.
- [25] Z.-Y. Xue, G.L. Schrader, *J. Phys. Chem. B* 103 (1999) 9459.
- [26] V.V. Guliants, J.B. Benziger, S. Sundaresan, N. Yao, I.E. Wachs, *Catal. Lett.* 32 (1995) 379.
- [27] A.D. Soejarto, G.W. Coulston, G.L. Schrader, *Can. J. Chem. Eng.* 74 (1996) 594.
- [28] G. Koyano, T. Okuhara, M. Misono, *J. Am. Chem. Soc.* 120 (1998) 767.